International Nano Letters (2018) 8:111–121
https://doi.org/10.1007/s40089-018-0234-6

ORIGINAL ARTICLE

Synthesis and characterization of polyvinyl pyrrolidone (PVP)-coated Fe_3O_4 nanoparticles by chemical co-precipitation method and removal of Congo red dye by adsorption process

Gajanan Pandey[1] · Sandhya Singh[1] · Gaurav Hitkari[1]

Received: 20 January 2018 / Accepted: 17 May 2018 / Published online: 25 May 2018

Abstract
The present paper deals synthesis of polyvinyl pyrrolidone (PVP)-coated magnetite nanoparticles by chemical co-precipitation method. The samples were characterized using X-ray diffraction, scanning electron microscopy, energy-dispersive X-ray spectroscopy (EDX), Fourier transform infrared spectroscopy (FT-IR) and Brunauer–Emmett–Teller (BET) methods. The surface area, pore volume and pore radius were calculated by the BET analysis. The EDX and FT-IR analysis demonstrated the fabrication of PVP-coated Fe_3O_4 NPs. The as-synthesized Fe_3O_4/PVP has successfully been used as an adsorbent for elimination of Congo red dye in aqueous medium.

Keywords Magnetite · Nanoparticles · Co-precipitation · Adsorption · BET · XRD · Electron microscopy

Introduction

Industrial effluent treatment is a provocative operation to restraint water contamination and to sustain ecosystem [1, 2]. Azo dyes are a renowned class of coloring compounds which are comprehensively been used in engineering applications. Congo red, a cationic dye, is benzidine derivative of azo dye and its structure is very stable. Even a slight concentration of the dye is revealed to be a foremost environmental threat [3, 4]. Exposure to MB leads to increase of heart beat, vomiting, shock, jaundice, quadriplegia, and tissue necrosis in humans [5, 6]. Various methods such as ultrafiltration, reverse osmosis, coagulation, sedimentation chemical oxidation, membrane separation processes, electrochemical, aerobic, anaerobic microbial degradation, etc. are accessible for waste water handling; however, these methods have limitations such as formation of inferior waste products which have to be further treated. Further, these procedures are time spending and price demanding [7–9]. In this regard, the adsorption procedure is an efficient approach to take out pollutants present in the effluent water. Since the water management by adsorption method is entirely dependent on excellence of the adsorbent, the improvement of effective and low-cost sorbent materials is challenging task before material chemists. In the previous years, number of adsorbents such as activated carbon, zeolites, clay minerals, chitosan, lignocelluloses, biosorbents and functionalized polymers have been employed; however, maximum of these materials are either not economic and effective or have associated difficulties of separation and generation of secondary wastes [10–14].

Due to large surface-to-volume ratio, nanomaterials are advanced class of adsorbent. In the recent years, iron oxide nanoparticles, especially magnetite (Fe_3O_4) and maghemite (γ-Fe_2O_3), are the frequently used magnetic importers in various biomedical applications such as magnetic resonance imaging, contrast development agents, hyperthermia, manipulating cell membranes, biosensors, cataloging, and in drug delivery [15]. The proficient, economic, accessible and non-toxic monodisperse synthesis of Fe_3O_4 nanoparticles is extremely preferred for potential environmental applications. Fe_3O_4 is a potential, inexpensive and effortlessly synthesizable adsorbent with additional benefit of ease of

✉ Gajanan Pandey
pandeygajanan@rediffmail.com

Sandhya Singh
sandhyacsjm011@gmail.com

Gaurav Hitkari
gauravbhu012@gmail.com

[1] Department of Applied Chemistry, Babasaheb Bhimrao Ambedkar Univesity (A Central University), Lucknow, UP 226025, India

solid–liquid separation using an external magnetic field. Debnath et al. reported the removal of an anionic organic dye (Congo red) using chemically synthesized Fe_2O_3 NPs as adsorbent and effect of pH, adsorbent dosage, temperature, adsorption time and primary concentration on adsorption was examined [16]. Saad et al. used sol–gel method to synthesize γ-Fe_2O_3-activated carbon nanocomposite for the selective removal of twofold mixture of dyes containing reactive red 223 dye (RR) and malachite green dye (MG) by ultrasonic-assisted adsorption method [17]. Nanosized magnetic iron oxide particles have been studied broadly as a novel adsorbent with great surface area and slight diffusion resistance by Shariati et al. [18]. In another report, magnetic iron oxide nanoparticles have been used for the elimination of dyes from artificial and actual textile wastewater using adsorption technique and the effect of different experimental parameters, viz. contact time, pH coexisting ions, was investigated [19]. Porous magnetic microspheres, synthesized by one-step Friedel–Crafts alkylation reaction, have been used for fast separation of dyes from aqueous solution [20]. Magnetite/reduced graphene oxide (MRGO) nanocomposites prepared via solvothermal approach have been developed to prepare for separation of dye waste product [21]. Further, the additional advantages such as ease of synthesis, recovery, nonexistence of secondary waste product, cost-effectiveness as well as environmental friendliness make these materials suitable candidates for effective treatment of effluent water [22].

Coprecipitation method is a cost effective, environmental friendly and biocompatible technique [23, 24]; however, ultra-small Fe_3O_4 nanoparticles have not been efficaciously prepared by this technique yet. Owing to large surface area and dipole–dipole interactions of magnetic nanoparticles have tendency to agglomerate, hence the challenging issue associated with the use of Fe_3O_4 nanoparticles as adsorbent is the stabilization. Polymers implanting on magnetic nanoparticles is unique attractive procedures of surface modification [25, 26]. In the number of previous reports, it has been shown the decoration of polymeric layer of lipids, proteins, dendrimers, gelatin, dextran, chitosan, poly (vinyl alcohol) (PVA), etc. over NPs can effectively stabilize magnetic nanoparticles [27–32]. Vadivel et al. demonstrated that PVP coating successfully controls structural, morphological, dielectric and magnetic properties of $CoFe_2O_4$ magnetic nanoparticles [33]. In this study, we used PVP polymer as coating material because it is water solvable, neutral, nonhazardous, and is frequently used in innumerable applications [34]. Since the polymer PVP is attached to magnetic nanoparticles by covalent bonds, the complete magnetic fluid (ferrofluid) becomes stable for an extensive age of time.

In present paper, we synthesized PVP-coated Fe_3O_4 nanoparticles via co-precipitation technique, structural and optical properties have been considered with respect to the variation in concentration of polymer and adsorption study has been examined for the elimination of Congo red dye from aqueous solution.

Experimental analysis

Materials required

All the chemicals used in this work were analytical grade and used as supplied. Ferric chloride hexa-hydrate ($FeCl_3{\cdot}6H_2O$), ferrous sulfate hepta-hydrate ($FeSO_4{\cdot}7H_2O$), polyvinyl pyrrolidone (PVP), ammonium hydroxide (NH_4OH, 26% of ammonia) and Congo red dye (CR) were procured from Merk. De-ionized water was used as solvent. All the glasswares were cleaned by concentrated acid. The dried apparatus was used in the completely experiments.

Synthesis of PVP-coated iron oxide nanoparticles

The PVP-coated Fe_3O_4 nanoparticles were fabricated by chemical co-precipitation method. In the typical experiment, 50 mL aqueous solution of 0.017 M of ferric chloride, 50 mL aqueous solution of 0.033 M of ferrous sulfate and 1 g polyvinyl pyrrolidone (PVP) were mixed in 250-mL lessened flask. The solution mixture was stirred for 30 min time to achieve a standardized solution. 0.25 M of ammonia solution was mixed in 50 mL of distilled water and added gradually to above solution mixture until pH reaches 11. The solution mixture was vigorously stirred on motorized stirrer for 3 h at room temperature. The solution appeared black color, which is symbolic of formation of Fe_3O_4. The precipitate was magnetically separated using an enduring magnet bar, liquefied in methanol and again separated by magnet bar. This process was repeated four times to remove the surplus amine molecules. Black powdered PVP-coated Fe_3O_4 nanoparticles were dried at room temperature for whole day time and calcinated at 400 °C for 4 h. In analogous way Fe_3O_4/PVP (2 g) and Fe_3O_4/PVP (3 g) materials were synthesized using 2 and 3 g PVP.

Batch adsorption studies

In this study, batch process was applied to estimate the adsorption process and the experiments were performed at room temperature (25 ± 1 °C) in 250-mL stoppered conical flask consisting of 50 mL solutions under study. In various adsorption experiments such as impact of pH on extent of adsorption, contact time for adsorption isotherm experiments, 40 mg of adsorbent Fe_3O_4/PVP (1 g) was assorted in 50 mL concentration of Congo red dye solutions. pH of the solutions was maintained by the addition of appropriate quantity of 0.1 M HCl and 0.1 M NaOH solutions. After

mixing of adsorbent into the investigation solution, beaker was shaken for a preferred contact time in an electrically thermostated reciprocating shaker at 150 rpm. To achieve the equilibrium condition, a proportion of solution was withdrawn at consistent time interval, centrifuged and investigated for residual Congo red using UV–Vis spectrophotometer (carry 100). The adsorption amount was calculated via the subsequent equation:

$$q = \frac{(C_0 - C_e)V}{m} \tag{1}$$

The sorption efficiency, A %, of the Congo red dye was calculated from:

$$A(\%) = \frac{(C_0 - C_e)V}{C_0}, \tag{2}$$

where C_0 and C_e are initial and equilibrium concentrations Congo red dye in mg/L, V is the volume of solution in mL and m is the amount of adsorbent in mg.

Characterization

The X-ray diffraction patterns of as-prepared PVP-coated Fe_3O_4 materials were observed on Pananalytical's X'Pert Pro X-ray diffractometer in the 2θ range 10–80° with step size of 0.025°. Scanning electron microscope (SEM) images of the products were carried out on JEOL 6490 LB equipment. The scanning electron microscopic images were attained at an operating electrical energy of 3 kV. FT-IR spectra of as-prepared Fe_3O_4/PVP (1 g), Fe_3O_4/PVP (2 g) and Fe_3O_4/PVP (3 g) samples were recorded on Perkin Elmer Spectrum two equipment. Brunauer–Emmett–Teller (BET) analysis of all the materials was carried out on BELSORP MINI (II) equipment. UV–Vis spectra were record in absorption mode with a carry 100 spectrophotometer in the 200–800 nm regions.

Results and discussion

XRD

To examine phase, crystal arrangement and purity of above-synthesized Fe_3O_4/PVP (1 g), Fe_3O_4/PVP (2 g) and Fe_3O_4/PVP (3 g) materials, XRD analysis was done and patterns are shown in Fig. 1a–c. The X-ray diffraction peaks in the XRD pattern of these materials are readily indexed as magnetite Fe_3O_4 phase. From the XRD pattern, it is evident that as-synthesized materials, obtained by calcination of precipitate at 400 °C for 3 h are phase pure Fe_3O_4. Furthermore, it is observable from the diffraction pattern that the XRD peaks are sharp and broadened; indicating formation of good crystalline and small sizes Fe_3O_4/PVP materials. The diffraction peaks

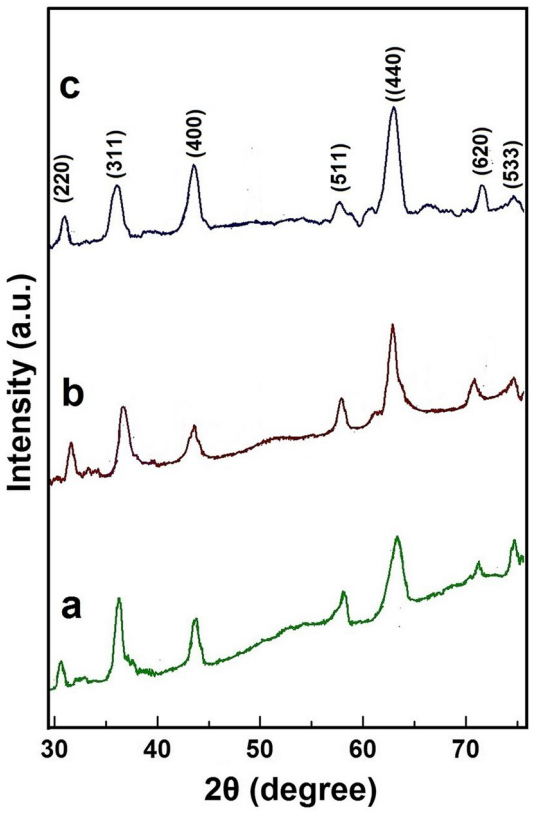

Fig. 1 XRD patterns of **a** Fe_3O_4/PVP (1 g), **b** Fe_3O_4/PVP (2 g), **c** Fe_3O_4/PVP (3 g) nanoparticles formed by calcination at 400 °C temperature

analogous to (311), (400), (511), (440), (620) and (533) are quite identical to distinguishing peaks of the Fe_3O_4 crystal with the cubic spinal structure.

Size of the crystal of Fe_3O_4/PVP (1 g), Fe_3O_4/PVP (2 g) and Fe_3O_4/PVP (3 g) materials was calculating using Scherer formula:

$$D = \frac{0.9\lambda}{\beta \cos\theta}, \tag{3}$$

where D is the crystallites size (in nm), λ the wavelength (in nm), β is the full width at half maxima (FWHM) and θ is the Bragg's diffraction angle.

Though Scherrer equation is approximate, however, it gives an idea about crystallites size, for the particle's dimension lower than 100 nm [35]. The width of diffraction peaks has contribution for the pair of instrumental and sample-dependent effects. To decouple overhead contributions, diffraction pattern from line widening of an accepted material (Al_2O_3) was collected to describe the instrumental broadening. The instrumental corrected β_{hkl} for a selected diffraction peak of the materials was calculated using the equation:

$$\beta_{hkl} = \left[\left(\beta_{hkl}^2\right) \text{measured} - \left(\beta^2\right) \text{instrumental}\right]^{1/2} \tag{4}$$

The XRD peak (311) was used to define average particle's size. The calculated average crystallite sizes of the materials Fe_3O_4/PVP (1 g), Fe_3O_4/PVP (2 g) and Fe_3O_4/PVP (3 g) were found to be 35, 32 and 30 nm, respectively.

FESEM and EDX

FESEM images (Fig. 2) indicate that the morphology of the Fe_3O_4 nanoparticles is roughly spherical in shape. As per reports, globular-shaped NPs form because the nucleation rate per unit area remains isotopic at the interface between the Fe_3O_4 magnetic nanoparticles [36, 37]. Figure 2a–c shows the typical FESEM micrographs of the samples Fe_3O_4/PVP (1 g), Fe_3O_4/PVP (2 g) and Fe_3O_4/PVP (3 g) which are of nano-aggregates of ultrafine particles. Agglomeration found in these samples is owing to the magnetic dipole–dipole interaction between NPs [38]. EDX pattern (Fig. 2d–f) shows the composition of elements present in

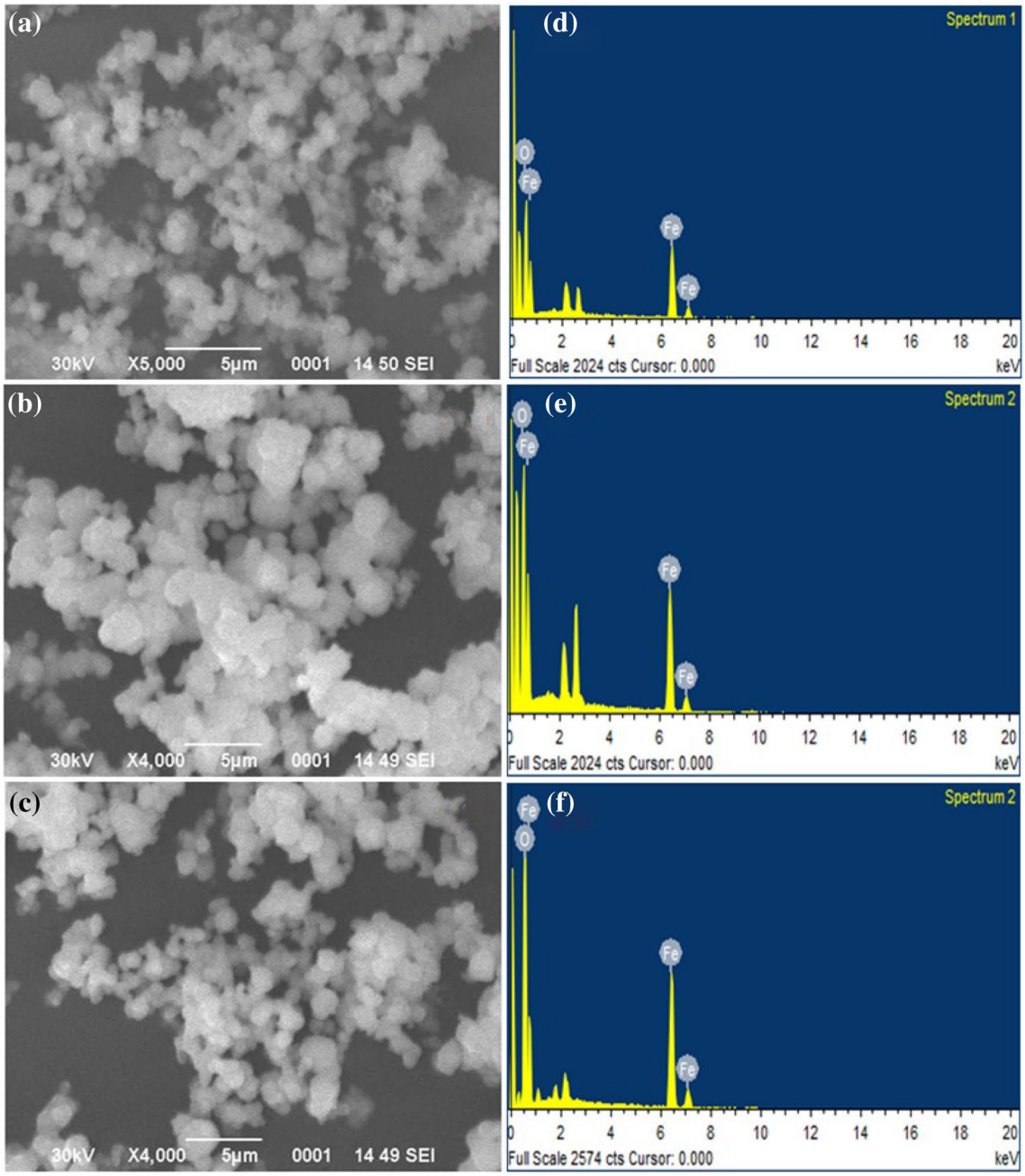

Fig. 2 The SEM image of **a** Fe_3O_4/PVP (1 g), **b** Fe_3O_4/PVP (2 g) and **c** Fe_3O_4/PVP (3 g) NPs. EDX pattern of **d** Fe_3O_4/PVP (1 g), **e** Fe_3O_4/PVP (2 g) and **f** Fe_3O_4/PVP (3 g) NPs

material. Strong peak of Fe and O was found in our sample and the percentage of Fe:O is found as 3:4.

FT-IR

The FT-IR spectra of Fe_3O_4 nanoparticles coated with disparate quantity of PVP are displayed in Fig. 3. In FT-IR spectra, one peak found in the range 3444–3401 cm^{-1} is owing to stretching frequency of –OH band of adsorbed water molecules on the surface of PVP-coated Fe_3O_4 NPs while the peaks obtained between 1615 and 1642 cm^{-1} in these samples are ascribed to stretching frequency of C=O. Two vibration bands perceived at 572 and 633 cm^{-1} in these samples are the frequencies of magnetite [39]. The one vibrational band at 572 cm^{-1} has been ascribed to IR-active T_{1u} mode of vibration in Fe_3O_4 nanoparticles [40]. On increasing the extent of PVP, the C=O absorption bands shifts as of 1680–1662 cm^{-1}. The results indication that iron oxide is bonded with carbonyl group in PVP and the interaction between PVP and Fe_3O_4 diminution of the particle size,

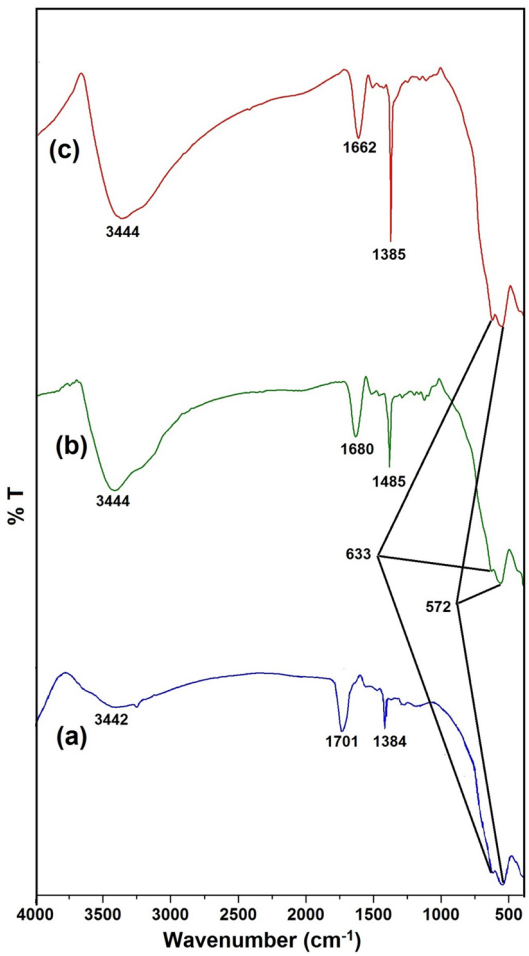

Fig. 3 FT-IR spectra of **a** Fe_3O_4/PVP (1 g), **b** Fe_3O_4/PVP (2 g), **c** Fe_3O_4/PVP (3 g)

which contribute to surface significance of nanoparticles. The peak situated at 1289 cm^{-1} is owing to C–N stretching vibration of *N*-vinyl pyrrolidone. Overall, these FT-IR spectra further validate the formation of magnetite NPs which are coated with PVP through C=O interaction.

BET

Nitrogen adsorption/desorption isotherm plots have been used to evaluate pore diameter (*D*p), pore volume (*V*p) and the surface area (*S*) of the synthesized materials in this study. The surface area of adsorbent material has immense significance in the adsorption process. Extra-large surface area is favorable for the adsorption procedure because then more active site is available for the adsorption of adsorbent. The isotherm profile of Fe_3O_4/PVP (1 g) indicates dissimilar porosity (a mixture of type IV and type II, according to IUPAC classification). While the samples Fe_3O_4/PVP (2 g) and Fe_3O_4/PVP (3 g) show a predominance of type IV with H_2 hysteresis loop. In example of sample Fe_3O_4/PVP (1 g), there is a high proportion of type II isotherms, the characteristic of mesoporous powders (H_4 hysteresis loop), which is fascinating for particular processes (catalysis and adsorption). The profile of pore diameter dissemination is presented in Fig. 4b (according to the BJH method revealed in Fig. 5) demonstrates a broad pore size distribution, with the mainstream of the porous diameter situated in the array from 0 to 100 A°. A rise in the quantity of iron in the sample composition stimulated variations in the hysteresis behavior, which can be accredited towards the closing of the pores by iron oxide. Table 1 presents detailed description of the standards of the surface area, overall pore volume, and the ordinary pore diameter of the samples, which point to the textural outcome, promoted by a rise in the extent of iron. Samples with higher iron amount seem to have a lesser ratio of left over organic substances after the calcination process.

Adsorption study

Effect of pH

The pH of the sorbent media governs charge of the surface of adsorbent, the degree of ionization and speciation of adsorbate which play critical role on the sorption capability [41]. In this study, the influence of pH on sorption of Congo red dye on the layer of Fe_3O_4/PVP (1 g) (40 mg) NPs was conducted at room temperature in the pH range 2–11. In the adsorption analysis, Fe_3O_4/PVP (1 g) was used as adsorbent because it showed sufficiently extraordinary surface area and the maximum pore volume among three materials. Desired pH was maintained by the addition 0.1 M HCl and 0.1 M NaOH solutions. The extent of adsorption of dye as a function of pH on the surface of Fe_3O_4/PVP (1 g) is depicted in

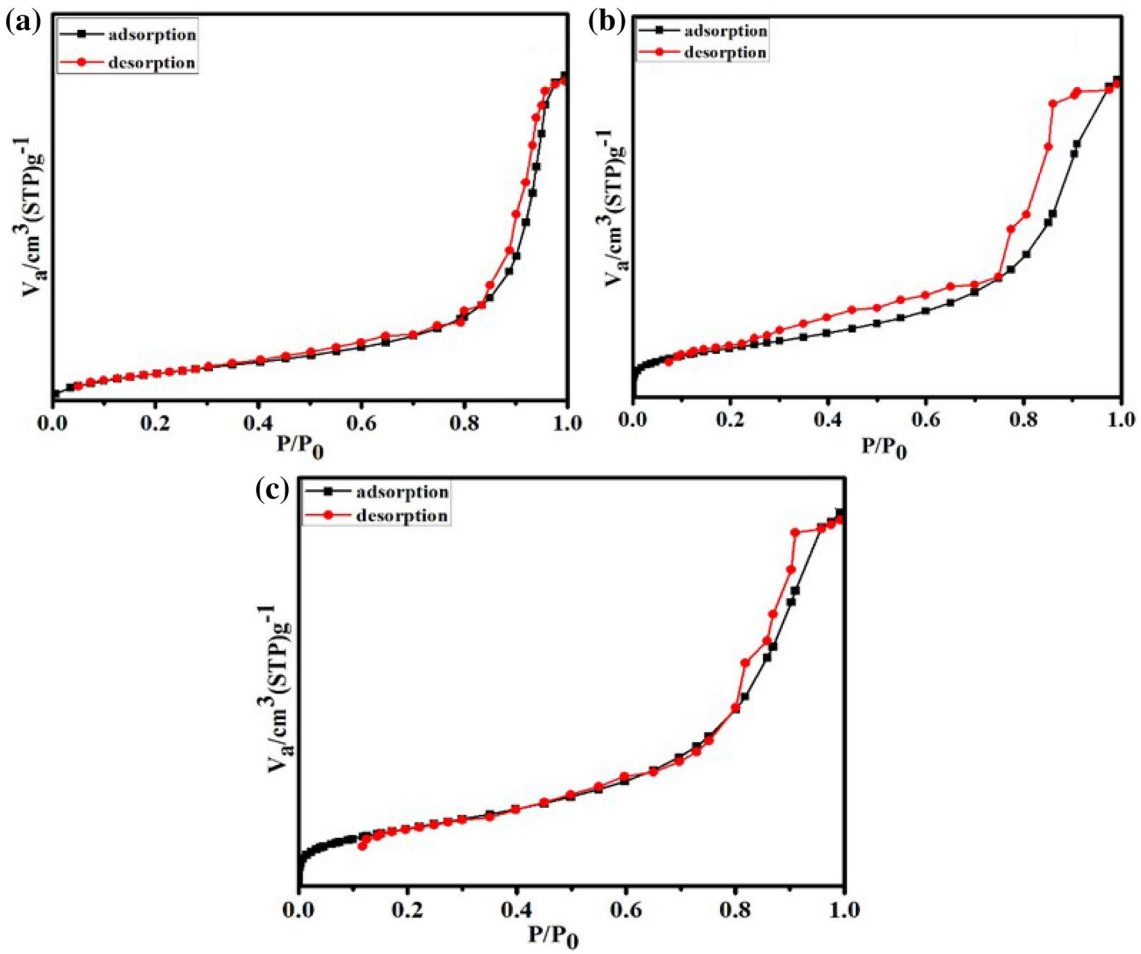

Fig. 4 N_2 adsorption–desorption isotherms of **a** Fe_3O_4/PVP (1 g), **b** Fe_3O_4/PVP (2 g), **c** Fe_3O_4/PVP (3 g) nanoparticles

Fig. 6. From the graph, it appears that the adsorption of dye is minimum at pH 2, rises with increase of pH and attains peak at pH 5. Thereafter, the extent of adsorption decreases, attains minima at pH 10 and become constant on further increase of pH.

Congo red dye is an anionic dye and releases anionic SO_3^- ions on dissociation, thus solution becomes alkaline in aqueous media. The extent of adsorption of these ions on the sorbent surface is first and foremost influenced by the surface charge of the adsorbent, which in turn depend on the solution pH. At low pH both, sorbent Fe_3O_4/PVP and dye Congo red, are highly protonated due to greater concentration and greater mobility of H^+ ions. Therefore, at low pH, the extent of adsorption of dye by surface of sorbent is low. On increasing the pH, the concentration of H^+ ions diminishes; therefore, Congo red dye removal increases and maxima achieved at pH 5, for the reason that of higher concentration of anionic charged ligand accessible for sorption. At higher pH (in alkaline medium), the sorbent Fe_3O_4/PVP is deprotonated and thus become reluctant to adsorption of negatively charged Congo red dye; therefore, the extent of dye adsorption decreases successively on increasing the pH up-to 10.

Effect of contact time

To evaluate the degree of dye adsorption by adsorbent Fe_3O_4/PVP (1 g) with course of time, series of tests were performed taking five Congo red dye concentrations, viz.,10, 20, 30, 40 and 50 ppm, at constant pH 6. The sorption studies were performed between 0 and 90 min in the time step of 10 min. The extent of Congo red adsorption took place rapidly as experiments commenced, however, it becomes slow later and attained plateau at equilibrium, which reached on 90 min of time. The uptake of Congo red dye was 12.03, 23.76, 35.43, 46.93, and 57.6 mg/g, respectively, for 10, 20, 30, 40 and 50 ppm sorbate solutions (Fig. 7). The equilibrium time for Congo red dye was 90 min for all five dye concentrations. From the curves, it is concluded that the equilibrium time does not depend on the initial concentration of Congo red.

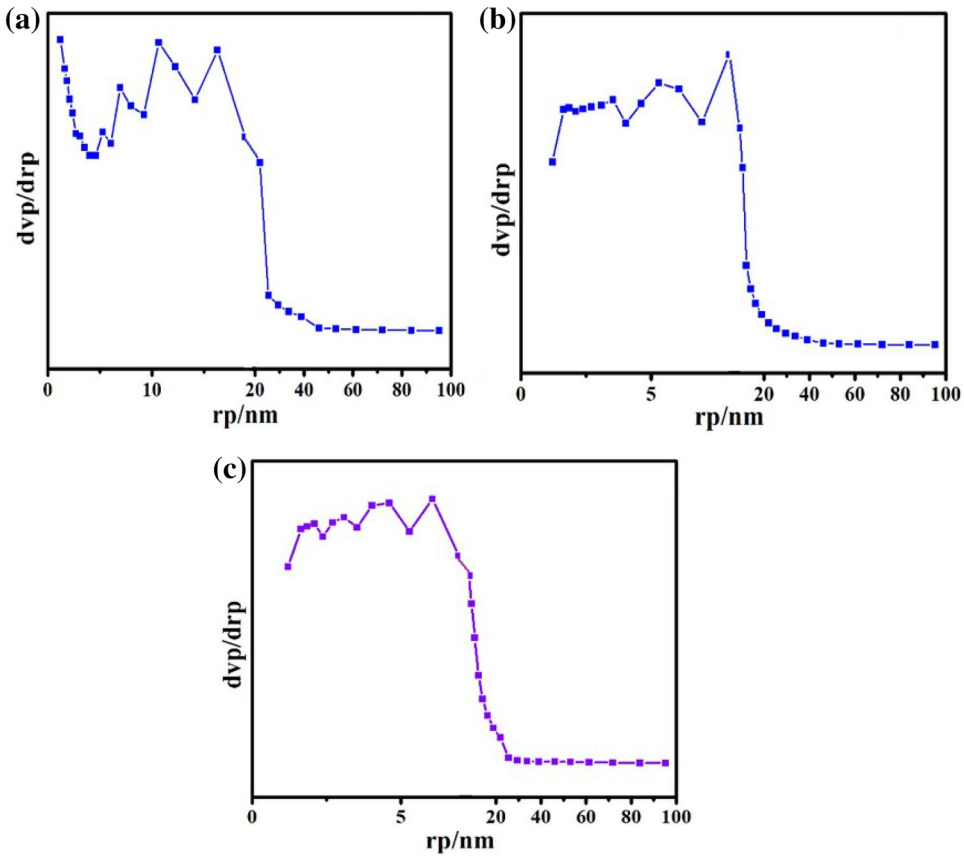

Fig. 5 BJH plot of **a** Fe_3O_4/PVP (1 g), **b** Fe_3O_4/PVP (2 g), **c** Fe_3O_4/PVP (3 g) NPs

Table 1 Values of the surface area, total pore volume, and the average pore diameter of the samples

Sample	S (m^2/gm.)	Vp (cm^2/gm.)	Dp (nm)
Fe_3O_4/PVP (1 g)	82.490	0.2991	1.21
Fe_3O_4/PVP (2 g)	110.94	0.2877	7.99
Fe_3O_4/PVP (3 g)	88.142	0.2128	6.06

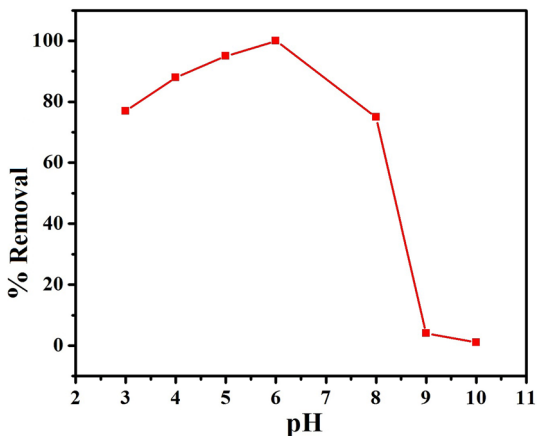

Fig. 6 Effect of pH on adsorption of Congo red dye on the surface of Fe_3O_4/PVP (1 g)

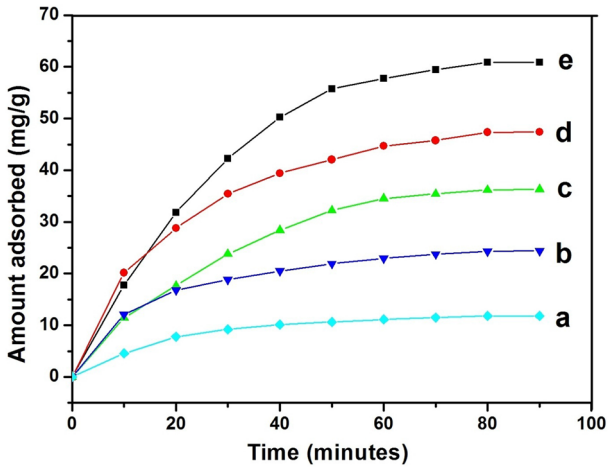

Fig. 7 Effect of contact time and initial metal ions concentration on adsorption Congo red dye on the surface of Fe_3O_4/PVP (1 g) at pH 6 on room temperature

Adsorption isotherm

With a view to explore the sorption mechanism at the surface of adsorbent Fe_3O_4/PVP (1 g), Langmuir and Freudlich isotherm models were examined for the

observed data. According to Langmuir sorption isotherm, the surface of sorbent is homogeneous and each sorption sites have equal sorbate affinity. Further, the adsorption at single site does not disturb sorption at neighboring cite [42] (Eq. 5).

$$\frac{C_e}{q_e} = \frac{1}{Q^0 b} + \frac{C_e}{Q^0} \tag{5}$$

Here, C_e is the equilibrium concentration (mg/L) of dye Congo red, q_e the quantity adsorbed per unit weight of sorbent adsorbent Fe_3O_4/PVP at equilibrium (mg/g), Q^0 (mg/g) and b is Langmuir constants, showing monolayer sorption ability and energy of sorption.

The Freundlich isotherm model defines the equilibrium at assorted surface and does not undertake monolayer formation. The equation in the linear for can be written as:

$$\log q^e = \log K_F + \frac{1}{n} \log C_e \tag{6}$$

In Eq. (6), n and K_F are Freundlich isotherm constants, representing concentration of sorption and relative sorption capability of sorbent. The n and K_F value can be calculated from the slope and intercept of the log qe versus log C_e plots.

Figure 8 shows the linear plots between C_e/qe versus C_e. Values of Langmuir constants Q^0 and b have been calculated from the slope and intercept of the graph (Table 2). Figure 9 indicates the Freundlich isotherm plots, log qe versus log C_e. The value of correlation coefficient R^2 was higher for Freundlich isotherm than that of Langmuir isotherm for Congo red dye, indicating suitable fitting of Freundlich isotherm is this study. Using Langmuir isotherm plot, the maximum sorption capacity of adsorbent Fe_3O_4/PVP for dye Congo red has been determined as 113.63 mg/g.

Table 2 Values of Langmuir and Freundlich sorption constants for removal of dye Congo red at pH 5 at room temperature

Langmuir isotherm model		Freundlich isotherm model	
R^2	0.9889	R^2	0.9946
Q^0 (mg/g)	113.63	n	1.41
b (L/mg)	0.2914	K_f	24.37

Sorption kinetics

In the batch adsorption experiment, Lagergren pseudo-first-order and pseudo-second-order kinetics models are the extensively used rate equations for determining the adsorption of solute from a liquid solution and these models have been used to understand the kinetics of present study. The Lagergren pseudo-first-order kinetics equation [43] can be expressed as:

$$\log (qe - qt) = \log qe - \frac{k1}{2.303} t \tag{7}$$

In Eq. (7) qe and q_t are amount of dye (mg/g) adsorbed at equilibrium and at time t, respectively, and k_1 is the rate constant of Lagergren pseudo-first-order sorption (min^{-1}). The qe and the value of rate constant k_1 have been calculated from the slope and intercepts of plots between log (qe − qt) versus t, as revealed in Fig. 10.

The kinetics data of dye adsorption have also been studied by pseudo-second-order equation [44]:

$$\frac{t}{qt} = \frac{1}{k_2 q_e^2} + \frac{1}{q_e} t \tag{8}$$

$$h = k_2' q_e^2, \tag{9}$$

where k_2 is the rate constant and h is the original adsorption rate. The rate constant k_2 and qe have been determined

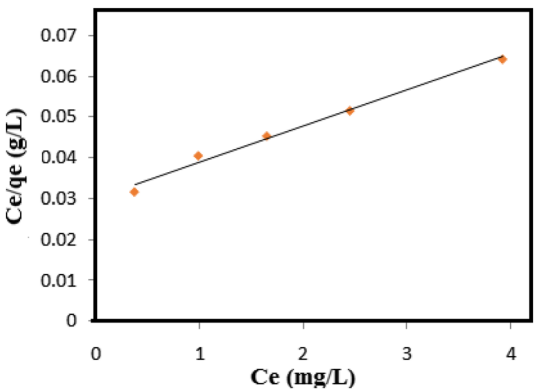

Fig. 8 Langmuir isotherm plot for adsorption Congo red dye on the surface of Fe_3O_4/PVP (1 g) at pH 6

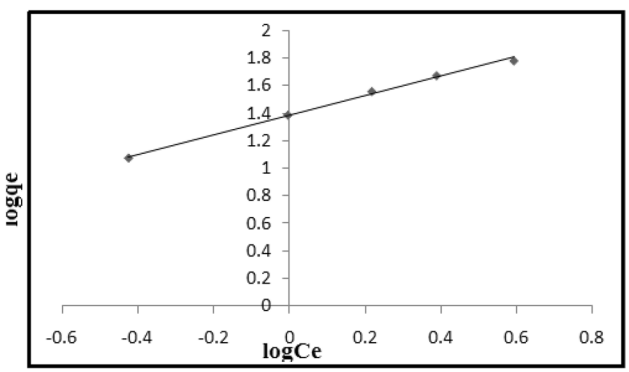

Fig. 9 Freundlich isotherm plot for adsorption Congo red dye on the surface of Fe_3O_4/PVP (1 g) at pH 6

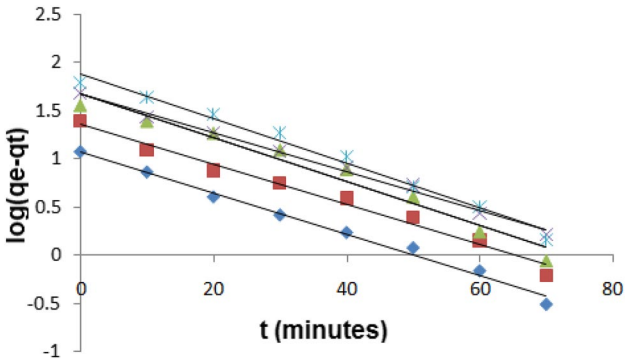

Fig. 10 Pseudo-first-order kinetics for adsorption Congo red dye on the surface of Fe_3O_4/PVP (1 g) at pH 6

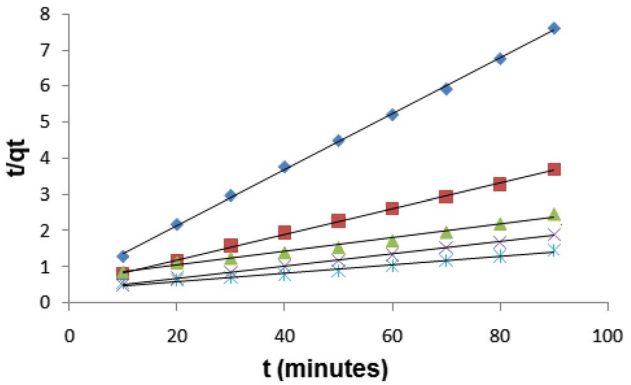

Fig. 11 Pseudo-second-order kinetics for adsorption Congo red dye on the surface of Fe_3O_4/PVP (1 g) at pH 6

from, respectively, slope and intercept *t*/qt against *t* plot (Fig. 11). The experimental values of qe, computed values of qe, rate constants and correlation constants (R^2) for both pseudo-first-order and pseudo-second-order equations are tabulated in Table 3. Closeness experimental and computed *qe* values for different kinetics models indicate their suitableness of rate kinetics [45]. Comparing the experimental and calculated qe values for pseudo-first-order and pseudo-second-order models, it has been found that the qe (exp.) and qe (calc.) values are more closer in instance of pseudo-first-order kinetics than pseudo-second order (Table 3), indicating former is suitable rate kinetics model. Correlation coefficient values (R^2) are very high for both pseudo-first and second-order kinetics models; however, these values are greater in situation of pseudo-second-order kinetics than the pseudo-first-order kinetics. Therefore, it has been resolved that the pseudo-second-order kinetics is the appropriate kinetics to reach the equilibrium for dye Congo red at the adsorbent Fe_3O_4/PVP surface.

Conclusion

Fe_3O_4 nanoparticles coated with varied amount of polyvinyl pyrrolidone (PVP) were successfully manufactured by a coprecipitation method. The synthesis route followed by calcination at 400 °C led to evolution of crystalline cubic inverse spinel structure Fe_3O_4/PVP nanoparticles with excellent adsorptive properties owing to high surface area and pore volume. Adsorption study performed using Fe_3O_4/PVP (1 g) as adsorbent since it showed high surface area and the highest pore volume. The highest adsorption was found at pH 6 using Fe_3O_4/PVP (1 g) as adsorbent. The equilibrium time for Congo red dye was 90 min and it is independent of the initial concentration of Congo red dye. The correlation coefficient R^2 was higher for Freundlich isotherm than that of Langmuir isotherm for Congo red dye, indicating Freundlich isotherm is suitable fitting in this study. Pseudo-second-order kinetics is the appropriate kinetics to reach the equilibrium for dye Congo red at the adsorbent Fe_3O_4/PVP surface. Therefore, it has been concluded that PVP-coated Fe_3O_4 NPs are effective adsorbent for the elimination of dye Congo red and hence it may be used for wastewater remediation on industrial scale.

Table 3 Comparison of pseudo-first-order and pseudo-second-order kinetic models for removal Congo red by Fe_3O_4/PVP (1 g) in different experimental conditions

Dye conc; C_0 (ppm)	Pseudo-first-order kinetics				Pseudo-second-order kinetics			
	qe (exp.) (mg/g)	qe (calc.) (mg/g)	K_1 (min^{-1})	R^2	Qe (calc.) (mg/g)	K_2 (g/mg/min)	*h* (mg/g/min)	R^2
10	11.82	11.80	0.0529	0.991	12.98	0.00999	1.67	0.999
20	24.38	22.69	0.0461	0.982	28.57	0.00243	1.98	0.999
30	36.31	39.81	0.0507	0.994	52.63	0.00054	1.48	0.987
40	47.40	47.53	0.0461	0.994	58.82	0.00087	3.02	0.999
50	60.91	76.03	0.0484	0.985	90.90	0.00032	2.63	0.991

References

1. Rocher, V., Siaugue, J.L., Cabuil, V., Bee, A.: Removal of organic dyes by magnetic alginate beads. Water Res. **42**, 1290–1298 (2008)
2. Tian, Y., Ji, C., Zhao, M., Xu, M., Zhang, Y., Wang, R.: Preparation and characterization of baker's yeast modified bynano-Fe_3O_4:application of biosorption of methyl violet in aqueous solution. Chem. Eng. J. **165**, 474–481 (2010)
3. Chen, S., Zhang, J., Zhang, C., Yue, Q., Li, Y., Li, C.: Equilibrium and kinetic studies of methyl orange and methyl violet adsorption on activated carbon derived from Phragmites australis. Desalination **252**, 149–156 (2010)
4. Murugesan, K., Kalaichelvan, P.: Synthetic dye decolourization by white rot fungi Indian. J. Exp. Bio. **41**, 1076–1087 (2003)
5. Kumar, K.V., Ramamurthi, V., Sivanesan, S.: Modeling the mechanism involved during the sorption of methylene blue on to fly ash. J. Colloid Interf. Sci. **284**, 14–21 (2005)
6. Uddin, M.T., Islam, M.A., Mahmud, S., Rukanuzzaman, M.: Adsorptive removal of methylene blue by tea waste. J. Hazard. Mater. **164**, 53–60 (2009)
7. Nasuha, N., Hameed, B., Din, A.T.M.: Rejected tea as a potential low-cost adsorbent for the removal of methylene blue. J. Hazard. Mater. **175**, 126–132 (2010)
8. Martin, M.J., Artola, A., Balaguer, M.D., Rigola, M.: Activated carbons developed from surplus sewage sludge for the removal of dyes from dilute aqueous solutions. Chem. Eng. J. **94**, 231–239 (2003)
9. Rauf, M., Qadri, S.M., Ashraf, S., Al-Mansoori, K.M.: Adsorption studies of toluidine blue from aqueous solutions onto gypsum. Chem. Eng. J. **150**, 90–95 (2009)
10. Shafeeyan, S.M., Daud, W.M.A.M., Houshm, A., Shamiri, A.: A review on surface modification of activated carbon for carbon dioxide adsorption. J. Anal. Appl. Pyrol. **89**, 143–151 (2010)
11. Panuccio, M.R., Sorgonà, A., Rizzo, M., Cacco, G.: Cadmium adsorption on vermiculite, zeolite and pumice: batch experimental studies. J. Environ. Manage. **90**, 364–374 (2009)
12. Hizal, J., Apak, R.: Modeling of cadmium (II) adsorption on kaolinite-based clays in the absence and presence of humic acid. Appl. Clay Sci. **32**, 232–244 (2006)
13. Bamgbose, J.T., Adewuyi, S., Bamgbose, O., Adetoye, A.A.: Adsorption kinetics of cadmium and lead by chitosan. Afr. J. Biotechnol. **9**, 2560–2565 (2010)
14. Panda, G.C., Das, S.K., Guha, A.K.: Biosorption of cadmium and nickel by functionalized husk of Lathyrussativus. Colloid Surf. B **62**, 173–179 (2008)
15. Gupta, A.K., Gupta, M.: Biomaterials synthesis and surface engineering of iron oxide nanoparticles for biomedical applications. Biomaterials **26**, 3995–4021 (2005)
16. Debnath, A., Deb, K., Das, N.S., Chattopadhyay, K.K., Saha, B.: Simple chemical route synthesis of Fe_2O_3 nanoparticles and its application for adsorptive removal of Congo red from aqueous media: artificial neural network modeling. J. Dispersion Sci. Technol. **37**, 775–785 (2016)
17. Muhammad, S., Tahir, H.: Synthesis of carbon loaded γ-Fe_2O_3 nanocomposite and their applicability for the selective removal of binary mixture of dyes by ultrasonic adsorption based on response surface methodology. Ultrason. Sonochem. **36**, 393–408 (2017)
18. Shahab, S., Khabazipour, M., Safa, F.: Synthesis and application of amine functionalized silica mesoporous magnetite nanoparticles for removal of chromium (VI) from aqueous solutions. J. Porous Mater. **24**, 129–139 (2017)
19. Nassar, N.N., Marei, N.N., Vitale, G., Arar, L.A.: Adsorptive removal of dyes from synthetic and real textile wastewater using magnetic iron oxide nanoparticles: thermodynamic and mechanistic insights. Can. J. Chem. Eng. **93**, 1965–1974 (2015)
20. Pan, L., Xu, M.Y., Liu, Z.L., Du, B.B., Yang, K.H., Wu, L., He, P., He, Y.J.: Facile method for the synthesis of Fe_3O_4@ HCP core–shell porous magnetic microspheres for fast separation of organic dyes from aqueous solution. RSC Adv. **6**, 47530–47535 (2016)
21. Hongmei, S., Cao, L., Lu, L.: Magnetite/reduced graphene oxide nanocomposites: one step solvothermal synthesis and use as a novel platform for removal of dye pollutants. Nano Res. **4**, 550–562 (2011)
22. Gupta, V.K., Nayak, A.: Cadmium removal and recovery from aqueous solutions by novel adsorbents prepared from orange peel and Fe_2O_3 nanoparticles. Chem. Eng. J. **180**, 81–90 (2012)
23. Mohapatra, S., Pramanik, N., Mukherjee, S., Ghosh, S.K., Pramanik, P.A.: simple synthesis of amine-derivatised superparamagnetic iron oxide nanoparticles for bioapplications. J. Mater. Sci. **42**, 7566–7574 (2007)
24. Zhang, Y., Wang, S.N., Ma, S., Guan, J.J., Li, D., Zhang, X.D., Zhang, J.D.: Self-assembly multifunctional nanocomposites with Fe3O4 magnetic core and CdSe/ZnS quantum dots shell. J. Biomedical Mater Res. A **85**, 840–846 (2008)
25. Fan, Q.L., Neoh, K.G., Kang, E.T., Shuter, B., Wang, S.C.: Solvent-free atom transfer radical polymerization for the preparation of poly (poly (ethyleneglycol) monomethacrylate)-grafted Fe_3O_4 nanoparticles: synthesis, characterization and cellular uptake. Biomaterials **28**, 5426–5436 (2007)
26. Yong, Y., Bai, Y., Li, Y., Lin, L., Cui, Y., Xia, C.: Preparation and application of polymer-grafted magnetic nanoparticles for lipase immobilization. J. Magn. Magn.Mater. **320**, 2350–2355 (2008)
27. Suh, W.H., Suslick, K.S., Stucky, G.D., Suh, Y.-H.: Nanotechnology, nanotoxicology, and neuroscience. Prog. Neurobiol. **87**, 133–170 (2009)
28. Kellar, K.E., Fujii, D.K., Gunther, W.H., Briley-Sæbø, K., Bjørnerud, A., Spiller, M., Koenig, S.H.: NC100150 injection, a preparation of optimized iron oxide nanoparticles for positive-contrast MR angiography. J. Mag. Reso. Imag. **11**, 488–494 (2000)
29. Zhao, X., Harris, J.M.: Novel degradable poly (ethylene glycol) hydrogels for controlled release of protein. J. Pharm. Sci. **87**, 1450–1458 (1998)
30. Jeong, Y.I., Nah, J.W., Na, H.K., Na, K., Kim, I.S., Cho, C.S., Kim, S.H.: Self-assembling nanospheres of hydrophobized pullulans in water. Drug Dev. Ind. Pharm. **25**, 917–927 (1999)
31. Massia, S.P., Stark, J., Letbetter, D.S.: Surface-immobilized dextran limits cell adhesion and spreading. Biomaterials **21**, 2253–2261 (2000)
32. Hao, R., Xing, R., Xu, Z., Hou, Y., Gao, S., Sun, S.: Synthesis, functionalization, and biomedical applications of multifunctional magnetic nanoparticles. Adv. Mater. **22**, 2729–2742 (2010)
33. Vadivel, M., Babu, R.M., Ramamurthi, K., Arivanandhan, M.: Effect of PVP concentrations on the structural, morphological, dielectric and magnetic properties of $CoFe_2O_4$ magnetic nanoparticles. NanoStruct. NanoObjects **11**, 112–123 (2017)
34. Garrec, D.L., Gori, S., Luo, L., Lessard, D., Smith, D., Yessine, M.-A., Ranger, M., Leroux, J.-C.: Poly (*N*-vinylpyrrolidone)-block-poly (D, L-lactide) as a new polymeric solubilizer for hydrophobic anticancer drugs: in vitro and in vivo evaluation. J. Control. Release **99**, 83–101 (2004)
35. Hitkari, G., Singh, S., Pandey, G.: Structural, optical and photocatalytic study of ZnO and ZnO-ZnS synthesized by chemical method. NanoStruct. NanoObjects **12**, 1–9 (2017)
36. Lu, W., Shen, Y., Xie, A., Zhang, W.: Green synthesis and characterization of superparamagnetic Fe_3O_4 nanoparticles. J. Magn. Magn. Mater. **322**, 1828–1833 (2010)

37. Kim, D.K., Mikhaylova, M., Zhang, Y., Muhammed, M.: Protective coating of superparamagnetic iron oxide nanoparticles. Chem. Mater. **15**, 1617–1627 (2003)
38. Jadhav, S., Nikam, D., Khot, V., Thorat, N., Phadatare, M., Ningthoujam, R., Salunkhe, A., Pawar, S.: Studies on colloidal stability of PVP-coated LSMO nanoparticles for magnetic fluid hyperthermia. New J. Chem. **37**, 3121–3130 (2013)
39. Cornwell, R.M., Schwertmann, U.: The iron oxides. Structure, properties, reactions, occurrences and uses, 2nd edn. Wiley VCH Gmbh & Co., Hoboken (2003)
40. Khalil, M.I.: Co-precipitation in aqueous solution synthesis of magnetite nanoparticles using iron(III) salts as precursors. Arab. J. Chem. **223**, 162–173 (2008)
41. El-Ashtoukhya, E.S.Z., Amina, N.K., Abdelwahabb, O.: Removal of lead(II) and copper(II) from aqueous solution using pomegranate peel as a new adsorbent. Desalination **223**, 162–173 (2008)
42. Singh, K.K., Rastogi, R., Hasan, S.H.: Removal of Cr(VI) from aqueous solutions using agricultural waste 'maize bran'. J. Hazard. Mater. **121**, 51–58 (2005)
43. Lagergren, S.: About the theory of so-called adsorption of soluble substances. Kungliga Svenska Vetenskapsakademiens Handlingar **24**, 1–39 (1898)
44. Ho, Y.S., McKay, G.: The kinetics of sorption of divalent metal ions onto sphagnum moss peat. Water Res. **34**, 735–742 (2000)
45. Febrianto, J., Kosasih, A.N., Sunarso, J., Ju, Y., Indraswati, N., Ismadji, S.: Equilibrium and kinetic studies in adsorption of heavy metals using biosorbent: a summary of recent studies. J. Hazard. Mater. **162**, 616–645 (2009)